

# Time Double-Slit Interference in Tunneling Ionization

D. G. Arbó<sup>†</sup>, E. Persson, and J. Burgdörfer

*Institute for Theoretical Physics, Vienna University of Technology,  
Wiedner Hauptstraße 8-10/136, A-1040 Vienna, Austria, EU and*

*<sup>†</sup>also at Institute for Astronomy and Space Physics,  
IAFE, CC 67, Suc. 28 (1428) Buenos Aires, Argentina*

(Dated: August 2, 2018)

We show that interference phenomena plays a big role for the electron yield in ionization of atoms by an ultra-short laser pulse. Our theoretical study of single ionization of atoms driven by few-cycles pulses extends the photoelectron spectrum observed in the double-slit experiment by Lindner et al, Phys. Rev. Lett. **95**, 040401 (2005) to a complete three-dimensional momentum picture. We show that different wave packets corresponding to the same single electron released at different times interfere, forming interference fringes in the two-dimensional momentum distributions. These structures reproduced by means of *ab initio* calculations are understood within a semiclassical model.

PACS numbers: 32.80.Rm,32.80.Fb,03.65.Sq

## I. INTRODUCTION

In the last years advanced laser facilities have achieved intensities of the order of  $10^{15} \text{W/cm}^2$  and pulse lengths of the order of 10 fs, which corresponds to few cycles of an electrical field of 800 nm wavelength [1]. The interaction process of such short and strong pulses with matter is a topic which has attracted much interest recently. Many experimental (see for example [2, 3]) and theoretical studies have been performed in this line. Theoretical calculations employ different methods: *ab initio* by solving the time dependent Schrödinger equation (TDSE) [4, 5, 6, 7]) or by using semiclassical approximation within the strong field approximation (SFA) methods [8, 9, 10], the (Coulomb-) Volkov approximation [11, 12], or by quasiclassical approximations where the electron is considered classically but the possibility of tunneling is incorporated within the WKB approximation [6, 13]. Very recent experiments show clear signs of interference among different parts of the wave packet detached at different times (different optical cycles of the electric field), when an external linear-polarized short-laser pulse is applied [18]. Clear interference peaks in the photoelectron spectra are observed in this kind of experiments. The photoelectron spectra of  $\text{He}^+$  for different angles of ejection are calculated in [19].

Another recent advance is the imaging of the momentum distribution of the ejected electron in ionization of rare-gas atoms by a moderately strong ultrashort laser pulse, in the transition regime from multiphoton to tunneling ionization. In single-electron emission [14], the longitudinal momentum distribution ( $k_z$  along the direction of the laser polarization) of photoelectrons from rare gases features a broad “double-hump” structure near threshold ( $E \simeq 0$ ) which surprisingly resembles the  $k_z$  distribution for non-sequential double ionization [3]. This structure is due to the interplay of the Coulomb interaction and laser field on the receding trajectory of the electron [3, 6, 16, 17]. A recently measured complex interference pattern near threshold in the two-dimensional mo-

mentum ( $k_z, k_\rho$ ) plane [14, 15] was also explained as near threshold Ramsauer-Townsend diffraction oscillations [7]. A simple semiclassical analysis identified the fringes resulting from interfering paths released at different times but reaching the same Kepler asymptote. Very recent experiments show clear signs of interference among different parts of the wave packet detached at different times (different optical cycles of the electric field), when an external linear-polarized short-laser pulse is applied [18]. Non-equispaced interference peaks in the photoelectron spectra are observed in this kind of experiments and calculations, for example the photoelectron spectra of  $\text{He}^+$  for different angles of ejection [19].

In this paper we generalize the study of interference in the energy (scalar) domain [18] to the momentum (vector) domain for the case of a 1-2 cycle pulse. We calculate the electron yield when a hydrogen atom is subject to a linear polarized two-cycles laser pulse with a  $\sin^2$  envelope function and show its similarity with a one-cycle pulse without envelope function. We demonstrate that non-equispaced peaks in the photoelectron spectrum stems from interference of different parts of the wave packets released at different times. Firstly, we solve the TDSE, then we make some classical considerations in order to intuitively understand the role of classical trajectories on interference phenomena, and lastly we present a semiclassical model which reproduce satisfactorily the calculated electron-yield distributions.

## II. THEORY AND RESULTS

We consider a hydrogen atom interacting with a linearly polarized laser field. The Hamiltonian of the system is

$$H = \frac{\vec{p}^2}{2} + V(r) + z F(t), \quad (1)$$

where  $V(r) = -1/r$  is the Coulomb potential energy,  $\vec{p}$  and  $\vec{r}$  are the momentum and position of the electron,

respectively, and  $\vec{F}(t)$  is the time dependent external field linearly polarized along the  $\hat{z}$  direction. The laser pulse is chosen to be of the form

$$\vec{F}(t) = \begin{cases} f(t) \sin(\omega t) \hat{z} & (0 \leq t \leq \tau) \\ \vec{0} & \text{otherwise} \end{cases}, \quad (2)$$

where  $\omega$  is the laser frequency,  $\tau$  the total pulse duration, and  $f(t)$  is the envelope function. Atomic units are used throughout.

### A. TDSE calculations

The time-dependent Schrödinger equation is solved by means of the generalized pseudo-spectral method [20]. The method combines a discretization of the radial coordinate optimized for the Coulomb singularity with quadrature methods to achieve stable long-time evolution using a split-operator method. It allows for an accurate description of both the unbound as well as the bound parts of the wave function  $|\psi(t)\rangle$ . The process of detecting an electron of momentum  $\vec{k}$  can then be viewed as a projection of the wave function onto the Coulomb wave functions [4, 21, 22]. Therefore, after the laser pulse is turned off, the wave packet is projected onto outgoing Coulomb wave functions which gives the asymptotic momentum distributions

$$\frac{dP}{d\vec{k}} = \frac{1}{4\pi k} \left| \sum_l e^{i\delta_l(k)} \sqrt{2l+1} P_l(\cos \theta_k) \langle k, l | \psi(\tau) \rangle \right|^2, \quad (3)$$

where  $\delta_l(k)$  is the momentum dependent Coulomb phase shift,  $\theta_k$  is the angle between  $\vec{k}$  and the polarization direction of the laser field,  $\hat{z}$ ,  $P_l$  is the Legendre polynomial of degree  $l$ , and  $|k, l\rangle$  is the eigenstate of the free atomic Hamiltonian with positive eigenenergy  $E = k^2/2$  and orbital quantum number  $l$ . The Coulomb projection is needed for the cases that a physical magnitude is not a constant of motion of the free evolution (once the external field is turned off), i.e., the components of the kinetic momentum. In turn, this is not the case for the photoelectron spectrum since the energy is a constant of motion of the free evolution. Cylindrical symmetry makes the dynamics a two dimensional problem, where the projection of the angular momentum on the polarization direction of the laser is a constant of motion (the magnetic quantum number  $m$  is unaffected during the time evolution). As the initial state of the system we consider the ground state of the Hydrogen atom, ( $m = 0$ ).

Firstly, a driving field of frequency  $\omega = 0.05$  with envelope function  $f(t) = F_0 \sin^2(\pi t/\tau)$ , peak field  $F_0 = 0.075$  corresponding to an intensity of  $2 \times 10^{14} \text{W/cm}^2$ , and time duration  $\tau = 251$  (which involves two complete optical cycles) is used. The inset of Fig. 1 (a) shows the pulse shape. The photoelectron spectrum, shown in Fig. 1 (a), has a non-equally spaced peaked structure, whose separation between two consecutive peaks increases with

energy. Recent simulations [19] have also shown the existence of these peaks in the density probabilities at different angles of ejection but for a much stronger field ( $10^{16} \text{Wcm}^{-2}$ ) applied to  $\text{He}^+$  atoms calculations.

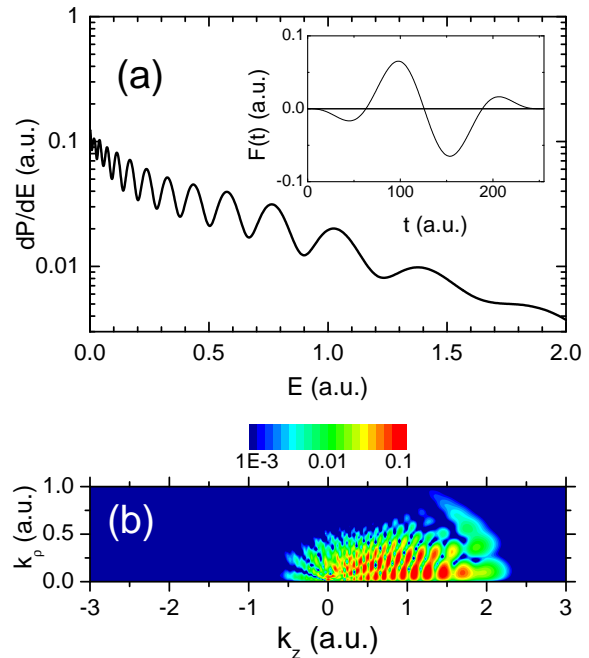


**FIG. 1:** (a) Photoelectron spectra for a two-cycle electric field of frequency  $\omega = 0.05$  a.u., peak field  $F_0 = 0.075$  a.u. and duration  $\tau = 4\pi/\omega = 251$ . Inset: Electric field as a function of time. (b) Doubly differential electron momentum distribution in cylindrical coordinates  $(k_z, k_\rho)$  in logarithmic scale for the same laser pulse.

In order to develop a more complete analysis we show in Fig. 1 (b) the double differential momentum distribution as a function of the final longitudinal  $-k_z$  and transversal  $-k_\rho = \sqrt{k_x^2 + k_y^2}$  momentum of the electron  $\frac{d^2P}{dk_\rho dk_z}$ . Different characteristics of the two-dimensional distribution are worth to be highlighted: (i) about the 95% of the distribution lies in the region of positive longitudinal momentum ( $k_z > 0$ ), (ii) more specifically the distribution is constrained to the region  $-0.5 \lesssim k_z \lesssim 2.5$  and  $k_\rho \lesssim 0.6$ , and the most important, (iii) a pattern with strip shape. It can also be observed some small radial structure for positive  $k_z$  near threshold. This kind of structure has recently been understood as generalized Ramsauer-Townsend type diffraction oscillations resulting from interfering paths released at different times [7].

In the following we consider a pulse with constant envelope function  $f(t) = F_0$  within  $[0, \tau]$  and 0 outside for two different values for the pulse duration:  $\tau = \pi/\omega = 63$

(half-cycle pulse) and  $\tau = 2\pi/\omega = 126$  (full-cycle pulse). In the case of the half-cycle pulse, the field, obviously, does not correspond to a traveling but to a standing wave [see Fig. 2 (a)]. We can observe the similarity of the shape of the one-cycle pulse of Fig. 2 (a), with the two-cycle pulse with envelope function in the inset of Fig. 1, where we can consider only one effective cycle (at the center) while the other is rather weak. As the pulse shapes of these two pulses are similar so should it also be the electron yield distributions.

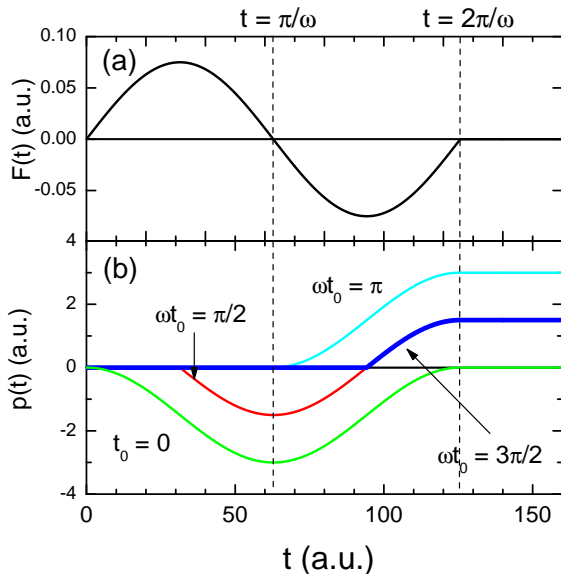


**FIG. 2:** (a) Electric field of frequency  $\omega = 0.05$ , duration  $\tau = 2\pi/\omega = 126$  a.u. and amplitude  $F_0 = 0.075$  a.u. as a function of time (1 cycle and square envelope function). (b) Kinetic momentum for different classical trajectories: electron detached at time  $t_0 = 0, \pi/2\omega, \pi/\omega, 3\pi/2\omega$ , and  $2\pi/\omega$ , as indicated. The momentum of the trajectories  $t_0 = \pi/2\omega$  and  $3\pi/2\omega$  coincide in the time interval  $t \geq 3\pi/2\omega$ .

In Fig. 3 (a) the photoelectron spectra for one-cycle pulse must be compared to the one of Fig. 1. In Fig. 3 (a) we showed the photoelectron spectra for a half-cycle and a full-cycle pulses are shown. The total ionization probability, which can be calculated as the integral of the energy distribution, is higher for a full cycle pulse than for a half cycle pulse, as expected. After half a cycle the ionization probability is 0.06, while after a full cycle pulse it is the double, 0.12. This shows that the system is in the linear ionization regime very far away from the saturation limit (depletion of the ground state). We will make use of this fact below, in subsection C. Both energy-distributions feature a peak structure with bigger separation between consecutive peaks as the energy increases. In turn, the photoelectron spectrum of a half-cycle pulse shows no oscillating structure. In Fig. 3 (b) the double-differential momentum distribution for a half-cycle shows

a complete smooth distribution in the negative longitudinal momentum  $-k_z$ - region. The pulse is not only responsible for the ionization of the atom but also for the motion of the wave packet towards the negative longitudinal momentum region. In turn, when a second half-cycle is included [Fig. 3 (d)] the whole wave packet moves towards the positive region and a clear fringe structure appears. This fact leads us to think that the peak structure of the one-cycle pulse spectrum emerges as a consequence of an interference effect. When considering a full cycle pulse, the wave packet created (released) during the first half cycle is pulled to the negative longitudinal momentum region after the first half cycle, but then is pulled towards the positive longitudinal momentum region by the second half-cycle. We observe that while the wave packet is spread about 3 a.u. in the positive longitudinal momentum, about only 0.5 a.u. (17%) in the transversal momentum. Additionally to the ionization in the first half cycle, another part of the wave packet appears in the continuum during the second half cycle which is also pulled towards the positive longitudinal momentum region. These two wave packets interfere, which can be observed in the double differential momentum distribution as clear interference fringes [Fig 3 (c)] and in the photoelectron spectrum as non-equispaced peaks [Fig. 3 (a)]. The spacing between the peaks increases with energy.

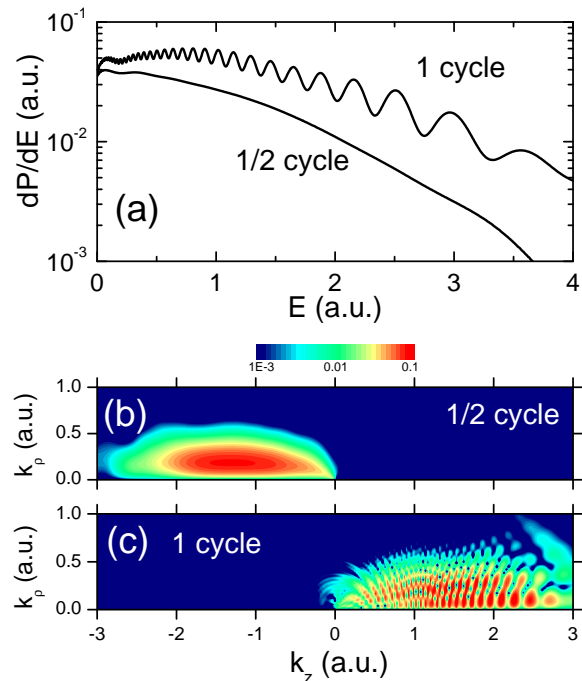


**FIG. 3:** (a) *Ab initio* photoelectron spectra for the case of the electric field in Fig. 2 (a): after a half-cycle pulse ( $\tau = \pi/\omega$ ) and one-cycle pulse ( $\tau = 2\pi/\omega$ ). (b) *Ab initio* doubly differential electron momentum distribution after the half-cycle pulse (one slit). (c) *Ab initio* doubly differential electron momentum distribution after the one-cycle pulse (two slits).

These interference processes can be reproduced with a simple semiclassical model of two electronic wave packets escaping from the nucleus near the extremes of the electric field and interfering in momentum space. We will see in subsection C that the mentioned interference process can be understood as the interference in momentum space of two electron classical trajectories escaping from the nucleus, one at each half cycle near the extremes of the electric field. We will give a clear analysis of this interference effect below by means of a semiclassical approach, but before a few classical considerations should be stated.

### B. Classical considerations

In this subsection we want to intuitively understand the physics of interference described in last subsection. We will see that it is sufficient to use a one-dimensional picture to glimpse the interference of the ionized atom. By using the classical equation of motion and considering the electron to detach from the nucleus at time  $t_0$  with zero velocity (Simple Man's Model [23]), it acquires the following (longitudinal) momentum

$$p(t) = \frac{F_0}{\omega} (\cos \omega t - \cos \omega t_0). \quad (4)$$

In Eq. (4), we make use of the strong field approximation (SFA), thus the effect of the atomic potential on the detached electron is neglected. The momentum  $p$  corresponds to the longitudinal momentum  $k_z$  in the three-dimensional case.

Most probably the atom is ionized at the extremes of the one-cycle electric field, i.e.,  $\omega t_0 = \pi/2$  and  $3\pi/2$ , thus Eq. (4) leads to  $p(t) = (F_0/\omega) \cos \omega t$ . Therefore, after a half-cycle pulse ( $\tau = \pi/\omega$ ) the momentum of the electron is  $p(t) = -F_0/\omega$ , and after a complete-cycle pulse ( $\tau = 2\pi/\omega$ ),  $p(t) = F_0/\omega$  [see Fig. 2 (b)]. In Fig. 3 (b) and (c) we can observe that the center of mass of the wave packet follows the classical quiver motion with amplitude  $F_0/\omega$ , i.e., right after the first half cycle it is negative,  $\langle k_z \rangle \simeq -F_0/\omega = -1.5$ , and right after the complete cycle it is positive,  $\langle k_z \rangle \simeq F_0/\omega = 1.5$ . The limit cases are trajectories of the electron released right at the beginning (or end) of the pulse  $t_0 = 0$  (or  $2\pi/\omega$ ) and right after the first half cycle ( $t_0 = \pi/\omega$ ). From Fig. 2 (b) [and from Eq. (4)] it can be easily seen that the momentum is constrained to values  $-2F_0/\omega < p < 0$ , right after a half-cycle pulse, and  $0 < p < 2F_0/\omega$ , right after a one-cycle pulse. In Fig. 3 (b) and (c) we observe that the quantum wave packets follow this classical constraint quite accurately.

In Fig. 2 (b) we see an example of two different trajectories released at times  $t_0 = \pi/2\omega$  and  $3\pi/2\omega$  having the same final momentum. It is straightforward from Eq. (4) to deduce that every pair of trajectories will have the

same final momentum  $p_1 = p_2$ , if their respective release times  $t_1$  and  $t_2$  accomplish with the relation

$$\omega(t_1 + t_2) = 2\pi. \quad (5)$$

This is exactly the condition for interference of two classical trajectories in the semiclassical model, as we will see in the next subsection.

In Fig. 2 we have considered only “direct electrons”, that is those which do not suffer any process of rescattering. In this one-dimensional model a rescattering process means an inversion of  $\pi$  in the scattering angle (change of sign in the momentum). Thus, the electrons would travel to the negative position direction,  $-z$ , instead of being expelled towards the positive direction after a complete cycle. As there are no other trajectories going in the  $-z$  direction, so there is no possibility of interference. Therefore, next these “indirect electrons” can be neglected for a one-cycle pulse and will be excluded from our semiclassical model of interference. This is not the case for a longer (more than one cycle) pulse where rescattering can occur in different cycles with the ensuing production of interference arising from indirect electron trajectories.

### C. Semiclassical model

Throughout this subsection we solve the TDSE under a set of approximations and will arrive to a simple analytical semiclassical solution [24]. These approximations, some of them already mentioned, are to be introduced throughout this subsection. We consider that there is only one atomic bound state ( $|0\rangle$ ) neglecting the bound excited states. In order to solve the Schrödinger equation with Hamiltonian given by Eq. (1) we assume the following ansatz

$$|\psi(t)\rangle = e^{iI_p t} \left[ a(t) |0\rangle + \int d\vec{v} b(\vec{v}, t) |\vec{v}\rangle \right], \quad (6)$$

where  $|\vec{v}\rangle$  is an eigenstate of the continuous spectrum with velocity  $\vec{v}$ , and  $I_p$  is the atomic ionization potential ( $I_p = 0.5$  for the hydrogen case). When we include Eq. (6) into the Schrödinger equation we arrive to the following expression for the amplitude of the continuum states:

$$b(\vec{k}, t) = - \sum_{i=1}^2 \left[ \frac{2\pi i F(t_{SP}^i)}{|\vec{k} + \vec{A}(t_{SP}^i)|} \right]^{1/2} d^*(\vec{k} + \vec{A}(t_{SP}^i)) e^{iS(t_{SP}^i, t)}, \quad (7)$$

where  $S$  accounts for the Volkov action,

$$S(t', t) = - \int_{t'}^t dt'' \left[ \frac{(\vec{k} + \vec{A}(t''))^2}{2} + I_p \right], \quad (8)$$

$d^*(\vec{v}) = \langle \vec{v} | z | 0 \rangle$  is the dipole element of the bound-continuum transition,  $\vec{A}(t) = - \int_0^t dt' \vec{F}(t')$  is the vector potential of the laser field divided by the speed

of light, and  $\vec{k}$  is the canonical momentum defined as  $\vec{k} = \vec{v}(t) - \vec{A}(t)$ . To arrive to Eq. (7) we have made use of  $\langle \vec{v} | \vec{v}' \rangle = \delta(\vec{v} - \vec{v}')$ , and the following approximations: (i) we neglect the depletion of the ground state ( $a(t) = 1$ ), (ii) continuum-continuum transitions are of the form  $\langle \vec{v} | z | \vec{v}' \rangle = i\nabla_v \delta(\vec{v} - \vec{v}')$ , and (iii) in order to get an analytical solution we apply the saddle-point approximation method [25].  $t_{SP}^i$  ( $i = 1, 2$ ) are the solutions of the stationary phase action

$$\frac{\partial S(t' = t_{SP}, t)}{\partial t'} = \frac{[\vec{k} + \vec{A}(t_{SP})]^2}{2} + I_p = 0. \quad (9)$$

The solutions of Eq. (9) are complex:

$$t_{SP}^1 = \frac{1}{\omega} \cos^{-1} \left[ 1 - \left( k_z \mp i\sqrt{2I_p + k_\rho^2} \right) \frac{\omega}{F_0} \right] \quad (10)$$

$$t_{SP}^2 = \frac{2\pi}{\omega} - t_{SP}^1.$$

Therefore, the sum in Eq. (7) must be understood as a two-term sum over the two different times  $t_{SP}^1$  and  $t_{SP}^2$  of Eq. (10). These two terms correspond to two different classical trajectories. The two ionization times in Eq. (10) accomplishes with the interference condition of Eq. (5).

Finally, the photoelectron spectrum can be written as  $\frac{dP}{dE} = 2\pi \int_{-1}^1 d \cos \theta_k \sqrt{2E} \left| b(\vec{k}, t = 2\pi/\omega) \right|^2$ , since the energy is a constant of motion of the free evolution (after the electric pulse is turned off), thus the energy distribution is invariant when taking the asymptotic limit  $t \rightarrow \infty$ . In this case, the kinetic momentum is not *a priori* invariant, but within the strong field approximation, once the electron is detached, it is not affected any longer by the core potential and, in consequence, the momentum distribution does not change when taking the limit  $t \rightarrow \infty$ . The momentum distribution  $\frac{dP}{dk} = \left| b(\vec{k}, t = 2\pi/\omega) \right|^2$  can be written as

$$\left| b(\vec{k}, t = 2\pi/\omega) \right|^2 = B(\vec{k}) \cos^2[\Delta S(\vec{k})] \quad (11)$$

where the phase  $\Delta S(\vec{k}) = S(t_{SP}^2, t) - S(t_{SP}^1, t)$  is responsible for the interference process, and the factor  $B(\vec{k})$  is the ionization probability at a time  $t_{SP}^i$  and states only for the modulation of the distribution of the unbound electrons. By making use of the simplified version of the saddle point method, where the ionization times of Eq. (10) are considered real (Simple Man's Model), the ionization probability can be written as [19]

$$B(\vec{k}) = \frac{\pi^2}{2(2I_p + k_\rho^2) |F(t(\vec{k}))|^2} \exp \left[ -\frac{2(2I_p + k_\rho^2)^{3/2}}{3|F(t(\vec{k}))|} \right]. \quad (12)$$

The reader can easily check that  $B(\vec{k})$  is invariant under the interchange  $t_{SP}^1 \leftrightarrow t_{SP}^2$  in Eq. (12), which is a

direct consequence of the assumption that no depletion of the ground state exists.

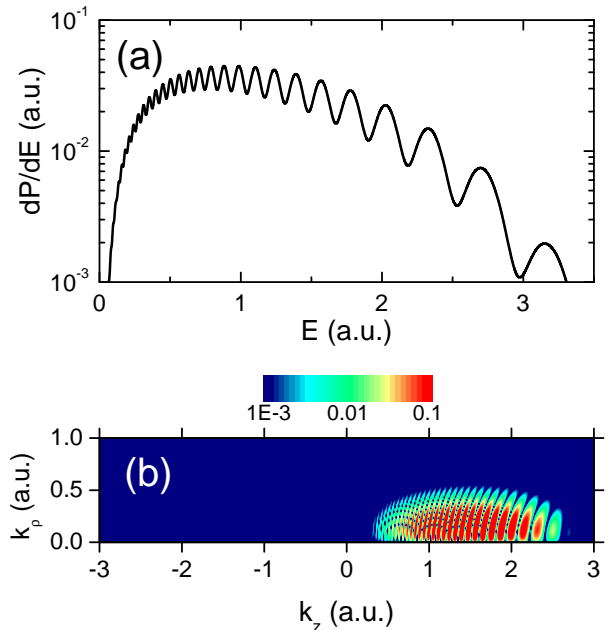


**FIG. 4:** (a) Semiclassical photoelectron spectrum corresponding to the field in Fig. 2 (a). (b) Semiclassical doubly differential electron momentum distribution after the pulse.

The results of the semiclassical model [Eq. (11)] are shown in Fig. 4. We observe a good qualitative agreement with the *ab initio* results of Fig. 3. The photoelectron spectrum calculated with the semiclassical model in Fig. 4 (a) reproduces the oscillating structure of the *ab initio* calculations in Fig. 3 (a), but the semiclassical model fails near threshold and in the high energy region (near classical boundaries). The same observation can be performed for the doubly differential momentum distributions in Fig. 4 (b) for the semiclassical model and Fig. 3 (c) for *ab initio* calculations. The interference pattern happens to be more complicated for *ab initio* calculations even though the semiclassical model reproduces the overall interference fringes. While the semiclassical distributions sticks (by construction) to the classical boundaries, the *ab initio* distribution invades a little bit the classically forbidden zone.

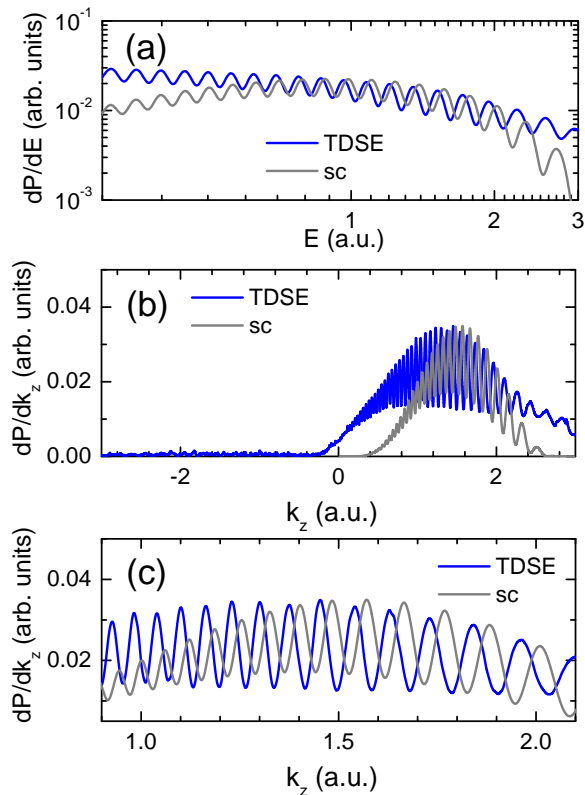


**FIG. 5:** (a) Photoelectron spectra by solving the TDSE and using the semiclassical (sc) model corresponding to the field in Fig. 2 (a). (b) Longitudinal momentum distributions by the two methods. (c) Zoom of Fig. (b) to show the agreement in separation between two consecutive peaks, even though there is a shift.

In order to perform a more quantitative comparison we show in Fig. 5 the results of both *ab initio* and semiclassical calculations. For this purpose, we have removed the excited bound states from the hydrogen spectrum in the quantum calculation (which is present in the semiclassical model). Therefore, the interference peaks in the photoelectron spectrum and the momentum distribution are more enhanced since they are not masked by the ionization coming from other bound states. Nevertheless, the distributions of Fig. 5 are very similar to the one with the full spectrum (Fig. 3). In Fig. 5 (a) we observed that for a long range of energies the agreement in the position of the peaks of the semiclassical energy spectrum and the TDSE one is very good. According to the classical mechanics [Eq. (4)] the energy spectrum is constrained to

$E < 2 \left(\frac{F_0}{\omega}\right)^2 = 4.5$  a.u. and, as mentioned before, we observe in Fig 5 (a) that the agreement is not so good near the extremes of the energy range, were the semiclassical spectrum decreases more abruptly. This feature is also observe for the longitudinal momentum distribution  $\frac{dP}{dk_z}$  in Fig. 5 (b). In most of the range the agreement is good as it can be seen in a zoom of the momentum distribution [Fig. 5 (c)], but it is not very good near the borders of the classical domain  $0 < k_z < \frac{2F_0}{\omega} = 3$  a.u., as expected according to the semiclassical theory. In both energy and momentum distribution the envelope function of Eq. (12) does not reproduce accurately the quantum results. Nevertheless, the interference pattern of ab initio calculations can be reproduced by the semiclassical model given by the second factor of Eq. (11). In figures 5 (a) and (c) the distance between two consecutive peaks is very similar in the two models but there is a shift in the position of the peaks of one model with respect to the other. This shift could be due to the effect of the coulomb potential on the ejected electron, which is present in the ab initio calculations but is neglected in the semiclassical model (SFA).

### III. CONCLUSIONS

In this article we have shown theoretical studies on the interference effects observed in the electron distributions of ionized hydrogen atoms subject to a linearly polarized short laser pulse. We have extended previous analysis in the energy domain to a full three-dimensional one in the momentum domain. The two-dimensional electron momentum distribution after a full cycle pulse evidences interference fringes. We have recognize the peak structure in the photoelectron spectrum and the longitudinal momentum distribution as the interference phenomenon between the wave packets released at the first and second half cycle, functioning each half cycle as an independent slit. In the understanding of the interference phenomenon we have made use of a simplified semiclassical model which has the advantage of being analytical. The semiclassical model reproduces quite well the interference patterns in the spectra of ejected electrons.

This work was supported by the SFB 016 ADLIS and the project P15025-N08 of the FWF (Austria), and by EU project HPRI-2001-50036. D.G.A. acknowledge support by Conicet of Argentina.

[1] G. G. Paulus *et al.*, Nature (London) **414**, 182 (2001); T. Brabec and F. Krausz, Rev. Mod. Phys. **72**, 545 (2000).  
 [2] G. G. Paulus *et al.*, Phys. Rev. Lett. **72**, 2851 (1994); G. G. Paulus *et al.*, J. Phys. B: At. Mol. Opt. Phys. **29**, L249-L256 (1996).  
 [3] R. Moshhammer *et al.*, Phys. Rev. Lett. **91**, 113002 (2003); R. Wiehle *et al.*, Phys. Rev. A **67**, 063405 (2003); J. Chen and C. H. Nam, Phys. Rev. A **66**, 053415 (2002); J. Chen

*et al.*, *ibid* **63**, 011404(R) (2000).

[4] S. Dionissopoulou *et al.*, Phys. Rev. A **55**, 4397 (1997).  
 [5] J. Wassaf *et al.*, Phys. Rev. A **67**, 053405 (2003).  
 [6] K. I. Dimitriou *et al.*, Phys. Rev. A **70**, 061404(R) (2004).  
 [7] D. G. Arb3, S. Yoshida, E. Persson, K. I. Dimitriou, and J. Burgd3rfer, Phys. Rev. Lett. **96**, 143003 (2006).  
 [8] N. B. Delone and V. P. Krainov, J. Opt. Soc. Am. B **8**, 1207 (1991).

- [9] Gerd van de Sand and Jan M. Rost, Phys. Rev. A **62**, 053403 (2000).
- [10] D. B. Milosevic, G. G. Paulus, and W. Becker, Optics Express **11**, 1418 (2003).
- [11] P. A. Macri, J. E. Miraglia, and M. S. Gravielle, J. Opt. Soc. Am. B **20**, 1801 (2003).
- [12] V. D. Rodriguez, E. Cormier, and R. Gayet, Phys. Rev. A **69**, 053402 (2004).
- [13] J. S. Cohen, Phys. Rev. A **64**, 043412 (2001); **68**, 033409 (2003).
- [14] A. Rudenko *et al.*, J. Phys. B **37**, L407-L413 (2004).
- [15] C. M. Maharjan, A.S. Alnaser, I. Litvinyuk, P. Ranitovic, and C. L. Cocke, J. Phys. B **39**, 1955 (2006).
- [16] F. H. M. Faisal and Schlegel, J. Phys. B **38**, L223 (2005).
- [17] J. Chen, J. Liu, L. B. Fu, and W. M. Zheng, Phys. Rev. A **63**, 011404(R) (2000).
- [18] Lindner *et al.*, Phys. Rev. Lett. **95**, 040401 (2005).
- [19] C. C. Chirila and R. M. Potvliege, Phys. Rev. A **71**, 031402(R) (2005).
- [20] X.-M. Tong and S. I. Chu, Chem. Phys. **217**, **119** (1997).
- [21] O. Schöller, J. S. Briggs, and R. M. Dreizler, J. Phys. B: At. Mol. Phys. **19**, 2505 (1986).
- [22] A. Messiah, *Quantum Mechanics 1* (North-Holland, New York, 1965); O. Schöller, *et al.*, J. Phys. B **19**, 2505 (1986); S. Dionissopoulou, *et al.*, Phys. Rev. A **55**, 4397 (1997).
- [23] P. B. Corkum, N. H. Burnett, and M. Y. Ivanov, Opt. Lett. **19**, 1870 (1994); M. Ivanov, P. B. Corkum, T. Zuo, and A. Bandrauk, Phys. Rev. Lett. **74**, 2933 (1994).
- [24] M. Lewenstein, K. C. Kulander, K. J. Schafer, and P.H. Bucksbaum, Phys. Rev. A **51**, 1495 (1995); M. Lewenstein, Ph. Balcau, M. Yu. Ivanov, Anne L'Huillier, and P. B. Corkum, Phys. Rev. A **49**, 2117 (1994).
- [25] Arfken, *Mathematical Methods for Physicist*, Academic Press Inc. (1985).